

Leaking Outside the Box: Kinetic Turbulence with Cosmic-Ray Escape

Evgeny A. Gorbunov^{1,*} Daniel Grošelj,¹ and Fabio Bacchini^{1,2}

¹*Centre for mathematical Plasma Astrophysics, Department of Mathematics, KU Leuven, Celestijnenlaan 200B, B-3001 Leuven, Belgium*

²*Royal Belgian Institute for Space Aeronomy, Solar-Terrestrial Centre of Excellence, Ringlaan 3, 1180 Uccle, Belgium*

We study particle acceleration in strongly turbulent pair plasmas using novel 3D Particle-in-Cell simulations, featuring particle injection from an external heat bath and diffusive escape. We demonstrate the formation of steady-state, nonthermal particle distributions with maximum energies reaching the Hillas limit. The steady state is characterized by the equilibration of plasma kinetic and magnetic pressures, which imposes upper limits on the acceleration rate. With growing cold plasma magnetization σ_0 , nonthermal power-law spectra become harder, and the fraction of energy channeled into escaping cosmic rays increases. At $\sigma_0 \gtrsim 1$, the escaping cosmic rays amount to more than 50% of the dissipated energy. Our method allows for kinetic studies of particle acceleration under steady-state conditions, with applications to a variety of astrophysical systems.

Introduction.—Turbulence is believed to be a widespread mechanism for nonthermal particle acceleration in collisionless plasmas [1–14]. In recent years, kinetic plasma simulations have provided first-principles insight into the mechanisms of particle acceleration in turbulent astrophysical environments by uncovering the nature of particle dynamics over their entire acceleration history [15–26]. It was shown that particles can be rapidly injected from the thermal pool into the suprathermal population by nonideal electric fields near reconnecting current sheets [19, 24, 27, 28]. The injection is followed by stochastic energization via interactions with turbulent structures [26, 29–33]. This can be seen as a generalization of the second-order Fermi process [1, 2, 34, 35], which involves diffusion in energy space.

However, most kinetic simulations to date face a significant shortcoming: they lack a genuine steady state, due to the fact that the simulation domains employed are of finite size and closed, which leads to a progressive accumulation of energy over time and to the pile-up of particles at the highest energies [17, 36, 37]. This presents challenges for connecting simulations and realistic astrophysical objects, which may convert a significant fraction of their available power into escaping cosmic rays. Moreover, it is known that power-law distributions emerge most naturally from a competition between particle acceleration and escape. In closed domains, the local trapping of particles provides an effective “escape” mechanism [36], enabling the development of power-law distributions. However, without an energy sink to balance the turbulent forcing, such power-law distributions are only transient states, followed by progressive energy pile-up. Therefore, steady-state simulations, if achievable, could offer a convenient and sorely needed testbed for theoretical models.

In this Letter, we develop an efficient method for achieving steady state in kinetic plasma-turbulence simulations in open domains, and we characterize the emerging steady-state statistics of particle acceleration and escape. As an example, we study large-amplitude 3D Alfvénic turbulence in electron–positron plasmas. The steady state is

characterized by a near-equilibration of plasma kinetic and magnetic pressures. As a result, bulk turbulent motions remain subrelativistic, which limits the rate of stochastic particle acceleration. The particle distributions exhibit nonthermal power laws extending up to the system size (Hillas) limit, where the rate of diffusive particle escape reaches the theoretical maximum (set by the light-crossing time). We also show that strongly magnetized sources may convert a large fraction of the available power into escaping cosmic rays. In our simulations, the nonthermal energy fraction of escaping particles grows with the cold plasma magnetization σ_0 (defined below) and saturates near 70% at $\sigma_0 \gtrsim 100$.

Kinetic Leaky-Box Model.—We perform 3D simulations of kinetic plasma turbulence with particle injection and escape using the Particle-in-Cell (PIC) code **Tristan-MP** v2 [38]. Our model mimics an open turbulent box of side $L = 2l_{\text{esc}}$, coupled to an external heat bath at a fixed temperature T_0 . Particles escape the magnetized turbulent accelerator by diffusing over a distance l_{esc} perpendicular to the mean magnetic field $\mathbf{B}_0 = B_0\hat{\mathbf{z}}$, while at the same time new thermal particles are introduced into the domain from the external heat reservoir. To implement escape, we introduce the particle variables δx and δy , which track the displacement of each particle from its initial location in x and y , respectively [39]. A particle counts as escaped when $\max(|\delta x|, |\delta y|) > l_{\text{esc}}$ (see also [25]). In order to keep the total number of particles fixed, we insert a new thermal particle (sampled from a Maxwellian at temperature T_0) at the location of every escaping particle. The inserted particle has the same charge and mass as the escaping particle.

Employing for simplicity an electron–positron composition ($m_{e^-} = m_{e^+} = m$) of mean number density n_0 , we explore the effect of different cold plasma magnetizations $\sigma_0 = B_0^2/(4\pi n_0 mc^2)$ on particle acceleration and escape. Several runs with different $\sigma_0 = \{0.2, 1, 4, 10, 20, 80\}$ are performed. A periodic box of size L^3 is initially filled with thermal particles at temperature T_0 . We set $T_0 = mc^2[\sigma_0(2 + \sigma_0)]/[3 + 3\sigma_0]$, which ensures that the

mean energy of the injected particles $E_0 \sim mc^2\sigma_0$ is close to the expected steady-state mean particle energy (see Eq. (1) below). To sustain turbulence, a Langevin antenna drives an external current [40] at the largest (box-scale) wavelengths with frequency $\omega_{\text{ant}} \approx 0.9\omega_A$, slightly off-resonant to the lowest Alfvén frequency of the box $\omega_A = (2\pi/L)v_A$. The Alfvén speed $v_A = c\sqrt{\sigma/(\sigma+1)}$ is defined here based on the initial hot magnetization $\sigma = B_0^2/(4\pi w_0 n_0 m c^2) = \sigma_0/w_0$, where $w_0 = \mathcal{K}_3(mc^2/T_0)/\mathcal{K}_2(mc^2/T_0)$ is the initial specific enthalpy and $\mathcal{K}_n(z)$ are n -th order modified Bessel functions of the second kind. The decorrelation rate of the antenna is $\gamma_{\text{ant}} = 0.5\omega_{\text{ant}}$. We focus on the strong-turbulence regime, where the magnetic perturbation driven by the antenna is comparable to the background magnetic field: $\delta B \equiv \delta B/B_0 \approx 1$. The spatial resolution of all simulations presented in this Letter is 960^3 , and the physical box size $L = 480d$, where $d = [(1+2\sigma_0)mc^2/(4\pi n_0 e^2)]^{1/2}$ is a reference hot-plasma skin depth based on the expected steady-state kinetic temperature (discussed below). We use 16 particles per cell in all runs [41]. The simulations are run for at least 20 light-crossing times $t_{\text{cross}} = l_{\text{esc}}/c$.

Energy Balance in Steady State.— Our simulations presented in the following show that large-amplitude kinetic turbulence with particle escape settles into a state where the average kinetic and magnetic pressures are of the same order. A supporting analytical argument can be provided by considering the balance between turbulent energization and energy losses from particle escape: $(E_{\text{esc}} - E_0)n_0/t_{\text{esc}} \simeq \delta b^2 B_0^2/(4\pi t_0)$, where E_{esc} is the mean energy of escaping particles, t_{esc} is the escape time, and t_0 is the turbulence cascade time. Assuming for simplicity that particles from the thermal population stream along tangled magnetic-field lines, thereby diffusing perpendicularly to the mean magnetic field, we estimate their escape time as $t_{\text{esc}} \simeq N\delta t \simeq l_{\text{esc}}^2/(l_{\parallel}\delta b^2 v_{\text{th}})$, where $\delta t \simeq l_{\parallel}/v_{\text{th}}$ is the time to travel one field-parallel correlation length l_{\parallel} at thermal speed $v_{\text{th}} \equiv [T/(wm)]^{1/2}$ and $N \simeq [l_{\text{esc}}/(l_{\parallel}\delta b)]^2$ is the number of correlation lengths needed to diffuse over a distance l_{esc} . The cascade time $t_0 \simeq \chi^{-2}l_{\parallel}/v_A \simeq l_0^2/(l_{\parallel}\delta b^2 v_A)$, where $\chi = \delta b l_{\parallel}/l_0$ is the turbulence nonlinearity parameter and l_0 is the perpendicular coherence scale. Focusing on the regime of interest with $\sigma_0 \gtrsim 1$, $(E_{\text{esc}} - E_0)/E_0 \gtrsim 1$, and assuming at most mildly relativistic Alfvén speeds, such that $v_A^2 \simeq c^2\sigma_0/w$ (to be justified below), we finally obtain

$$\beta \sim (\delta b l_{\text{esc}}/l_0)^{4/3}, \quad (1)$$

where $\beta \simeq 2v_{\text{th}}^2/v_A^2 \simeq 2T/(\sigma_0 mc^2)$ is the plasma beta, i.e., the ratio of plasma kinetic to magnetic pressures. Thus, large-amplitude ($\delta b \sim 1$) magnetized turbulence, driven on scales comparable to the particle escape distance ($l_0 \sim l_{\text{esc}}$), naturally settles into a state with $\beta \sim 1$. This enforces an upper limit on the hot plasma magnetization $\sigma \lesssim 1$, thereby limiting the turbulent motions $\delta v \simeq \delta b v_A$ to the mildly relativistic regime. In turn, this limits

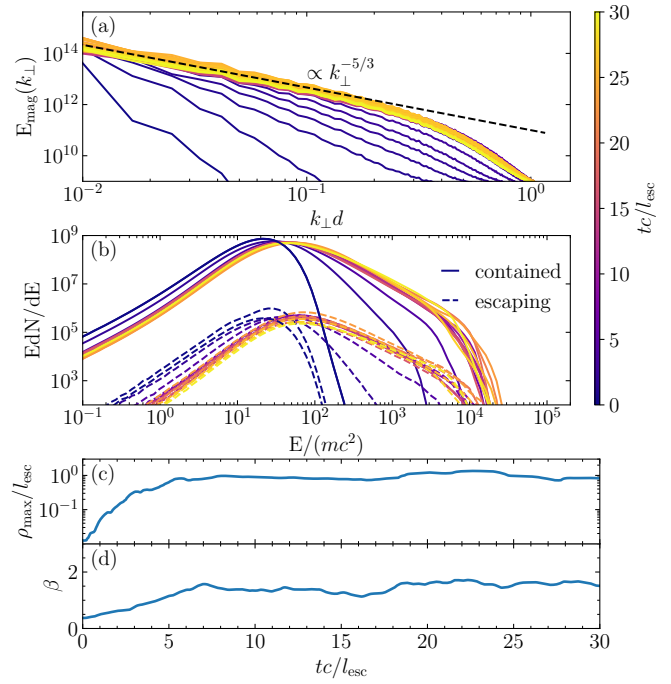


Figure 1. Approach toward steady state at $\sigma_0 = 20$. (a) Evolution of magnetic-field spectra (colors represent time). The dashed line shows a $-5/3$ slope for reference. (b) Temporal evolution of the particle energy spectra. Escaping-particle spectra are shown with dashed lines, contained with solid lines. (c) The Larmor radius $\rho_{\text{max}}(t)$ of the highest-energy particles. (d) Evolution of the plasma $\beta \equiv 8\pi n_0 T/B_{\text{rms}}^2$ over time.

the maximum particle scattering rate and the resulting acceleration efficiency, as shown below.

Simulation Results.— In Fig. 1 we demonstrate the formation of a self-consistent steady state in our kinetic leaky-box model, using the $\sigma_0 = 20$ case as an example. The temporal evolution of the 1D magnetic spectrum $E_{\text{mag}}(k_{\perp})$ as a function of the field-perpendicular wave number k_{\perp} is shown in Fig. 1(a). A steady-state turbulence spectrum is obtained after $\approx 5l_{\text{esc}}/c$. At magnetohydrodynamic (MHD) scales ($k_{\perp}d \ll 1$), the spectrum follows a familiar scaling $\propto k_{\perp}^{-5/3}$ [42], contrary to recent theoretical expectations [43] arguing that nonlinear cosmic-ray feedback leads to a significant steepening of the MHD turbulence spectrum. The formation of steady-state nonthermal particle distributions is depicted in Fig. 1(b). The initially Maxwellian energy distribution develops nonthermal features at high energies, characterized by a power-law dependence $f(E) \equiv dN/dE \propto \gamma^{-p}$. For $\sigma_0 = 20$, the power-law index reaches a mean value of $p \approx 2.8$ after ≈ 7 light-crossing times. The presence of escape allows us to measure the distribution of the escaping particles $f_{\text{esc}}(E)$, which develops a slightly harder power-law tail, saturating at an index $p \approx 2.5$.

In Fig. 1(c), we track the evolution of the Larmor radius $\rho_{\text{max}} = (\gamma_{\text{max}}^2 - 1)^{1/2}mc^2/(qB_0)$ of the highest-energy

particles in the box [44]. As appropriate for $\delta b \sim 1$, we assume that the highest-energy particles have large pitch angles [19]; for $\delta b \ll 1$ the (small) pitch angle should be included in the estimate of ρ_{\max} [45, 46]. At early times, $\rho_{\max}(t)$ in Fig. 1(c) grows at near-exponential rate [26], which is followed by saturation at the Hillas limit $\rho_{\max} \approx \rho_{\text{Hillas}} \approx l_{\text{esc}}$. The energization of the plasma and its approach toward steady state is evident also from the evolution of the plasma-beta parameter $\beta \equiv 8\pi n_0 T / B_{\text{rms}}^2$ (Fig. 1(d)), where $T = [mc^2/(3n_0)] \int (\gamma - 1/\gamma) f(E) dE$ and $\gamma \equiv E/(mc^2) + 1$ [47]. From panel (d) of Fig. 1, we can conclude that the average $\beta \approx 1.5$ in steady state. This is a generic feature of all of our runs: for any value of the cold magnetization σ_0 , the system eventually relaxes toward a state in which the plasma kinetic and magnetic pressures equilibrate, in line with the theoretical argument presented above. Such a universal behavior at high magnetization introduces an upper limit on the bulk turbulent motions of the plasma. Since the hot magnetization $\sigma = \sigma_0/w \approx 0.33$ (where we used $w \approx 4T/(mc^2) \approx 3\sigma_0$), the typical Alfvén speed is $v_A \approx 0.5c$, implying that the bulk motions are at most mildly relativistic, at least in the absence of radiative-cooling mechanisms [16, 22, 25].

How the plasma magnetization σ_0 shapes the nonthermal particle distributions is shown in Fig. 2. Fig. 2(a) shows the steady-state particle distributions as a function of $E/(\sigma_0 mc^2)$. Due to the linear dependence $T \propto \sigma_0 mc^2$ (see Eq. (1)), the distribution peaks approximately overlap, albeit with a slight shift toward lower energies for higher σ_0 . Efficient acceleration is enabled in all cases considered, in the sense that all distributions form extended nonthermal tails reaching the maximum energy set by the system-size (Hillas) limit ($\rho_{\max} \approx l_{\text{esc}}$; marked with star symbols in panel (a)). More strongly magnetized systems feature harder nonthermal tails, as shown in the inset of Fig. 2(a). The obtained power-law slopes are broadly consistent with previous kinetic simulations of strong turbulence in closed domains [15, 19, 22, 23, 27].

In Fig. 2(b) we show the fraction of particles and of the kinetic energy contained in nonthermal (i.e., non-Maxwellian) particles. The nonthermal population is defined as $f_{\text{nt}} = f(E) - f_M(E)$, where $f_M(E)$ is a Maxwellian distribution fitted with the data below the peak of $f(E)$. The fraction of energy contained in nonthermal particles exceeds 50% at $\sigma_0 \gtrsim 1$. Therefore, our results show that strongly magnetized turbulent accelerators can release a large fraction of the dissipated power into escaping cosmic rays (i.e., into nonthermal particles). At $\sigma_0 \gtrsim 100$ the escaping cosmic rays amount to about $\approx 20\%$ of the particles leaving the box and they carry away $\approx 70\%$ of the dissipated turbulence power. Finally, we confirm that the steady-state plasma β is remarkably independent of σ_0 and maintains a value $\beta \approx 1.5$ in all simulations, as shown in Fig. 2(c), in line with our analytical expectation.

In strongly magnetized turbulence, particles can be injected into the nonthermal population at reconnecting

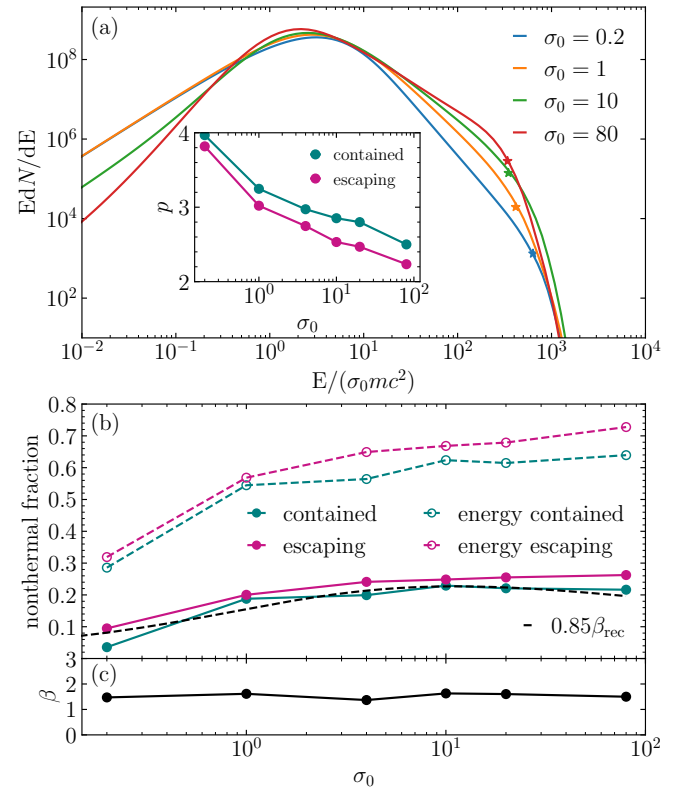


Figure 2. (a) Steady-state particle distributions of the contained population. Stars denote the Hillas limit. The inset shows the measured power-law indices for both contained (green line) and escaping (pink line) particle populations. (b) The number fraction of nonthermal particles (solid lines) and the fraction of energy attributed to nonthermal particles (dashed lines) for the contained (green) and escaping (pink) population. (c) The measured steady-state plasma β for different cold magnetizations σ_0 . For simulations with $\delta b < 1$ see Appendix A.

current sheets [19]. Following the reconnection scenario, we can estimate the fraction of nonthermal particles ξ_{nt} from the expected rate of reconnection in relativistic plasmas [48]. In one turbulence eddy turnover time, reconnecting sheets process a fraction $\mathcal{V}_{\text{rec}} \sim \beta_{\text{rec}}$ of the plasma volume [19], where β_{rec} is the reconnection rate in units of $B_0 v_A$, assuming $\delta B \sim B_0$ (i.e., moderate-guide-field reconnection). The reconnection rate can be obtained from the slope S of the separatrix field lines (defining the reconnection exhaust) as $\beta_{\text{rec}} \simeq S(1 - S^2)/(1 + S^2)$ [48–50]. Following [48], we express [51]:

$$S^2 = 1 - \frac{[2 + \sigma_m/2](1 + S^2)/(1 - S^2) - 1}{[1 + \sigma_m/2]\{1 + (\sigma_m/2)(1 - S^2)/(1 + S^2)\}^{1/2}}, \quad (2)$$

where $\sigma_m \approx \sigma_0(1 - S^2)/(1 + S^2)$ is the “microscale” magnetization parameter, and we took half of the asymptotic X-line kinetic pressure to obtain the above formula [48]. Assuming that an order-unity fraction of particles reprocessed by reconnection is injected into the acceleration

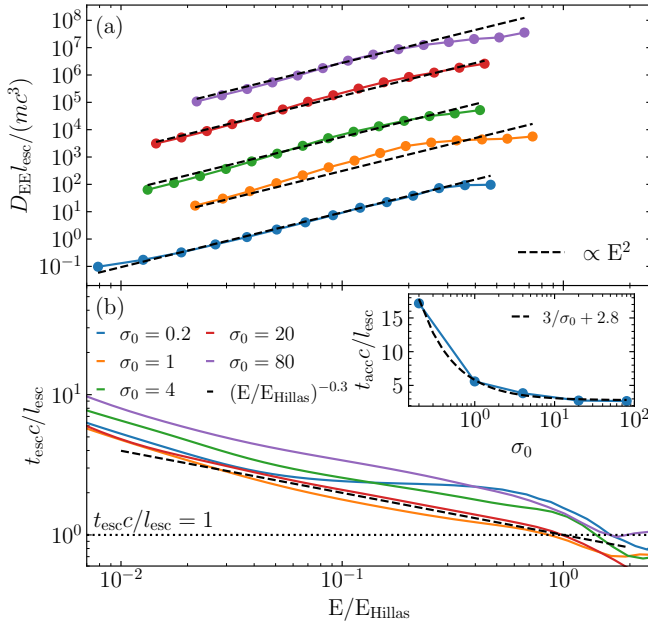


Figure 3. (a) Energy diffusion coefficient versus energy for different σ_0 . Dashed black lines indicate fits of the form $D_{EE} = E^2/t_{acc}$, where t_{acc} is the acceleration time. (b) Escape time t_{esc} versus energy for different σ_0 . The inset shows the acceleration time $t_{acc}(\sigma_0)$, which is well-described by a fit of the form $t_{acc}c/l_{esc} \approx 3/\sigma_0 + 2.8$.

process [52], we finally estimate the nonthermal fraction as $\xi_{nt} \sim \beta_{rec}$. Our estimate $\xi_{nt} \approx 0.85\beta_{rec}$ (with 0.85 as an ad hoc prefactor) is shown with a black dashed line in Fig. 2(b), demonstrating good agreement with the simulations. We note that particles need not be injected exclusively by the nonideal electric fields at reconnecting current sheets [53]; different forms of injection are still debated (e.g., [28, 54]). In particular, with decreasing σ_0 the effect of nonideal fields is expected to diminish, as the particles become less magnetized.

In Fig. 3, we study the statistics of particle acceleration and escape. We obtain the acceleration time scale t_{acc} by measuring the energy diffusion coefficient $D_{EE}(E)$ [19, 20], which defines the acceleration time as $t_{acc}(E) = E^2/D_{EE}(E)$. To this end, we track simulation particles located in different energy bins starting from a time t_* [55], and we obtain the energy-diffusion coefficient as $D_{EE}(E) = \langle \Delta E(t)^2 \rangle / \Delta t$, where $\Delta E(t) = E(t) - E(t_*)$, $\Delta t = t - t_* \approx l_{esc}/c$, and the angular brackets represent an average over all particles in a given energy bin. The dependence of diffusion coefficients on energy for different magnetizations is shown in Fig. 3(a). The diffusion coefficients scale as $D_{EE} \propto E^2$, consistent with previous measurements performed in closed domains [19, 20]. A slight departure from the $\propto E^2$ scaling is seen at high energies, approaching the Hillas limit. By performing fits of the form $D_{EE}(E) = E^2/t_{acc}$ (dashed black lines), we determine the acceleration time $t_{acc}(\sigma_0)$ (inset of Fig. 3(b)).

The efficiency of acceleration is related to the speed of the scattering agents [34], which typically move with the velocity of the turbulent bulk flow $\delta v \sim v_A$. The rate of stochastic acceleration is then limited by the largest achievable steady-state bulk velocity. This is reflected in our fitting formula $t_{acc} \approx (3/\sigma_0 + 2.8)l_{esc}/c$. For $\sigma_0 \gg 1$, the acceleration time settles at $t_{acc} \approx 2.8l_{esc}/c$, which represents the asymptotic value set by the heating-regulated ceiling for the Alfvén speed.

We define the escape time based on the energy-dependent flux of escaping particles (e.g., [56]) as $t_{esc} = f(E)/f_{esc}(E)$, where $f_{esc}(E)$ is the number of particles leaving the box per unit of energy and per unit time. The measured $t_{esc}(E)$ are shown in Fig. 3(b). An approximate fitting formula is $t_{esc} \approx (E/E_{Hillas})^{-0.3}l_{esc}/c$. The -0.3 exponent is consistent with existing literature [24, 31, 32]. Note that for the moderate-magnetization case ($\sigma_0 = 0.2$), t_{esc} is instead approximately constant in the nonthermal tail. A lower limit on the escape time is imposed by the light-crossing time l_{esc}/c (dotted horizontal line in Fig. 3(b)). We observe that this limit is approximately reached at the highest energies, corresponding to the Hillas limit, which reflects the fact that the highest-energy particles are not confined by the accelerator and thus escape via ballistic motion.

Discussion.—We conducted the first PIC simulations of kinetic turbulence with diffusive particle escape. Our method allows us to study the self-consistent production of cosmic rays in *true* steady-state turbulence, which was never achieved before in fully kinetic simulations of turbulent plasmas. Our novel approach has potential applications to a variety of moderately to strongly magnetized astrophysical objects, such as pulsar wind nebulae [57–60], jets from supermassive black holes [61–63], and accretion disks in active galactic nuclei [64–66]. As an example, we focused on 3D simulations employing a pair-plasma composition. We have demonstrated the formation of steady-state nonthermal particle distributions featuring extended power-law tails reaching the system size (Hillas) limit. The nonthermal power-law index p hardens with the cold plasma magnetization σ_0 . At $\sigma_0 \gg 1$, our results indicate an asymptotic value of $p \approx 2.3$ and $p \approx 2$ for the contained and escaping particle populations, respectively. The steady state is characterized by the equilibration of plasma kinetic and magnetic pressures ($\beta \approx 1$). This effect constrains the magnitude of turbulent bulk motions to subrelativistic speeds, which imposes limits on the maximum acceleration rate. This means that the acceleration time under steady-state conditions is bounded from below when $\sigma_0 \gg 1$. In our simulations, the lower bound is at $t_{acc} \approx 2.8l_{esc}/c$. We also measure the energy-dependent escape time and find that $t_{esc} \approx (E/E_{Hillas})^{-0.3}l_{esc}/c$.

Our numerical experiments also show that strongly magnetized turbulent accelerators can release a large fraction of the dissipated power into escaping cosmic rays, which can then feedback on the ambient medium. At

$\sigma_0 \gg 1$, the nonthermal particles (i.e., cosmic rays) carry up to $\approx 70\%$ of the total escaping energy flux. Such a large amount of energy contained in the nonthermal tail might provide nonlinear feedback on the turbulent cascade itself [43]; contrary to expectations, we do not observe any significant modification of the turbulence spectrum in our simulations, and this aspect warrants further investigation.

E.A.G. acknowledges useful discussions with M. Lemoine, A. Philippov, and V. Zhdankin during the development of this work. D.G. thanks L. Comisso and L. Sironi for stimulating discussions, which motivated this study. F.B. acknowledges support from the FED-tWIN programme (profile Prf-2020-004, project “ENERGY”) issued by BELSPO, and from the FWO Junior Research Project G020224N granted by the Research Foundation – Flanders (FWO). D.G. is supported by the Research Foundation – Flanders (FWO) Senior Postdoctoral Fellowship 12B1424N. The resources and services used in this work were provided by the VSC (Flemish Supercomputer Center), funded by the Research Foundation - Flanders (FWO) and the Flemish Government.

* genegorbs@gmail.com

- [1] E. Fermi, On the Origin of the Cosmic Radiation, *Phys. Rev.* **75**, 1169 (1949).
- [2] E. Fermi, Galactic Magnetic Fields and the Origin of Cosmic Radiation., *Astrophys. J.* **119**, 1 (1954).
- [3] R. M. Kilpua and A. Ferrari, The relativistic quasilinear theory of particle acceleration by hydromagnetic turbulence, *Astrophysics and Space Science* **12**, 302 (1971).
- [4] R. Ramaty, Energetic particles in solar flares, *AIP Conference Proceedings* **56**, 135 (1979).
- [5] C. D. Dermer, J. A. Miller, and H. Li, Stochastic Particle Acceleration near Accreting Black Holes, *Astrophys. J.* **456**, 106 (1996).
- [6] S. Liu, V. Petrosian, and F. Melia, Electron Acceleration around the Supermassive Black Hole at the Galactic Center, *The Astrophysical Journal* **611**, L101 (2004).
- [7] G. Brunetti and A. Lazarian, Compressible turbulence in galaxy clusters: physics and stochastic particle reacceleration, *Monthly Notices of the Royal Astronomical Society* **378**, 245 (2007).
- [8] V. Petrosian and W. E. East, Heating and Acceleration of Intracluster Medium Electrons by Turbulence, *The Astrophysical Journal* **682**, 175 (2008).
- [9] S. O’Sullivan, B. Reville, and A. M. Taylor, Stochastic particle acceleration in the lobes of giant radio galaxies, *Monthly Notices of the Royal Astronomical Society* **400**, 248 (2009).
- [10] V. Petrosian, Stochastic Acceleration by Turbulence, *Space Science Reviews* **173**, 535 (2012).
- [11] J. W. Lynn, E. Quataert, B. D. G. Chandran, and I. J. Parrish, Acceleration of relativistic electrons by magnetohydrodynamic turbulence: Implications for non-thermal emission from black hole accretion disks, *The Astrophysical Journal* **791**, 71 (2014).
- [12] S. S. Kimura, K. Toma, T. K. Suzuki, and S.-i. Inutsuka, Stochastic particle acceleration in turbulence generated by magnetorotational instability, *The Astrophysical Journal* **822**, 88 (2016).
- [13] A. Sciaccaluga and F. Tavecchio, Extreme TeV BL Lacs: a self-consistent stochastic acceleration model, *Monthly Notices of the Royal Astronomical Society* **517**, 2502 (2022).
- [14] V. Zhdankin, Non-thermal particle acceleration from maximum entropy in collisionless plasmas, *Journal of Plasma Physics* **88**, 175880303 (2022).
- [15] V. Zhdankin, G. R. Werner, D. A. Uzdensky, and M. C. Begelman, Kinetic Turbulence in Relativistic Plasma: From Thermal Bath to Nonthermal Continuum, *Phys. Rev. Lett.* **118**, 055103 (2017).
- [16] V. Zhdankin, D. A. Uzdensky, G. R. Werner, and M. C. Begelman, Numerical investigation of kinetic turbulence in relativistic pair plasmas – I. Turbulence statistics, *Monthly Notices of the Royal Astronomical Society* **474**, 2514 (2017).
- [17] V. Zhdankin, D. A. Uzdensky, G. R. Werner, and M. C. Begelman, System-size Convergence of Nonthermal Particle Acceleration in Relativistic Plasma Turbulence, *The Astrophysical Journal Letters* **867**, L18 (2018).
- [18] V. Zhdankin, D. A. Uzdensky, G. R. Werner, and M. C. Begelman, Electron and Ion Energization in Relativistic Plasma Turbulence, *Phys. Rev. Lett.* **122**, 055101 (2019).
- [19] L. Comisso and L. Sironi, The Interplay of Magnetically Dominated Turbulence and Magnetic Reconnection in Producing Nonthermal Particles, *The Astrophysical Journal* **886**, 122 (2019).
- [20] K. Wong, V. Zhdankin, D. A. Uzdensky, G. R. Werner, and M. C. Begelman, First-principles Demonstration of Diffusive-advection Particle Acceleration in Kinetic Simulations of Relativistic Plasma Turbulence, *The Astrophysical Journal Letters* **893**, L7 (2020).
- [21] V. Zhdankin, Particle Energization in Relativistic Plasma Turbulence: Solenoidal versus Compressive Driving, *The Astrophysical Journal* **922**, 172 (2021).
- [22] C. Vega, S. Boldyrev, V. Roytershteyn, and M. Medvedev, Turbulence and Particle Acceleration in a Relativistic Plasma, *The Astrophysical Journal Letters* **924**, L19 (2022).
- [23] C. Vega, S. Boldyrev, and V. Roytershteyn, Spatial Intermittency of Particle Distribution in Relativistic Plasma Turbulence, *The Astrophysical Journal* **949**, 98 (2023).
- [24] L. Comisso, G. R. Farrar, and M. S. Muzio, Ultra-High-Energy Cosmic Rays Accelerated by Magnetically Dominated Turbulence, *The Astrophysical Journal Letters* **977**, L18 (2024).
- [25] D. Grošelj, H. Hakobyan, A. M. Beloborodov, L. Sironi, and A. Philippov, Radiative Particle-in-Cell Simulations of Turbulent Comptonization in Magnetized Black-Hole Coronae, *Phys. Rev. Lett.* **132**, 085202 (2024).
- [26] C. Vega, S. Boldyrev, and V. Roytershteyn, Particle Acceleration in Relativistic Alfvénic Turbulence, *The Astrophysical Journal* **971**, 106 (2024).
- [27] L. Comisso and L. Sironi, Particle Acceleration in Relativistic Plasma Turbulence, *Phys. Rev. Lett.* **121**, 255101 (2018).
- [28] L. Sironi, Nonideal Fields Solve the Injection Problem in Relativistic Reconnection, *Phys. Rev. Lett.* **128**, 145102 (2022).
- [29] V. Bresci, M. Lemoine, L. Gremillet, L. Comisso, L. Sironi,

and C. Demidem, Nonresonant particle acceleration in strong turbulence: Comparison to kinetic and MHD simulations, *Phys. Rev. D* **106**, 023028 (2022).

[30] O. Pezzi, P. Blasi, and W. H. Matthaeus, Relativistic Particle Transport and Acceleration in Structured Plasma Turbulence, *The Astrophysical Journal* **928**, 25 (2022).

[31] P. Kempfki, D. B. Fielding, E. Quataert, A. K. Galishnikova, M. W. Kunz, A. A. Philippov, and B. Ripperda, Cosmic ray transport in large-amplitude turbulence with small-scale field reversals, *Monthly Notices of the Royal Astronomical Society* **525**, 4985 (2023).

[32] M. Lemoine, Particle transport through localized interactions with sharp magnetic field bends in MHD turbulence, *Journal of Plasma Physics* **89**, 175890501 (2023).

[33] S. Xu and A. Lazarian, Turbulent Reconnection Acceleration, *The Astrophysical Journal* **942**, 21 (2022).

[34] M. Lemoine, Generalized Fermi acceleration, *Phys. Rev. D* **99**, 083006 (2019).

[35] M. Lemoine, Effective theory for stochastic particle acceleration, with application to magnetized turbulence, *Phys. Rev. E*, (2025).

[36] M. Lemoine and M. A. Malkov, Power-law spectra from stochastic acceleration, *Monthly Notices of the Royal Astronomical Society* **499**, 4972 (2020).

[37] K. W. Wong, V. Zhdankin, D. A. Uzdensky, G. R. Werner, and M. C. Begelman, Energy Diffusion and Advection Coefficients in Kinetic Simulations of Relativistic Plasma Turbulence, *arXiv e-prints*, arXiv:2502.03042 (2025).

[38] H. Hakobyan, A. Spitkovsky, A. Chernoglazov, A. Philippov, D. Groselj, and J. Mahlmann, *Princetonuniversity/tristan-mp-v2: v2.6* (2023).

[39] Particles inserted at $t > 0$ are initialized with $\delta x = \delta y = 0$ (i.e., the reference point for the displacement is the particle's own initial location). For particles in the box at $t = 0$ we make an exception. Their initial δx and δy are preset to random numbers between $-l_{\text{esc}}$ and l_{esc} , as if those particles had already dispersed from their point of origin.

[40] J. TenBarge, G. Howes, W. Dorland, and G. Hammett, An oscillating Langevin antenna for driving plasma turbulence simulations, *Computer Physics Communications* **185**, 578 (2014).

[41] For a convergence check in particle number, see e.g. [19].

[42] P. Goldreich and S. Sridhar, Toward a Theory of Interstellar Turbulence. II. Strong Alfvénic Turbulence, *Astrophys. J.* **438**, 763 (1995).

[43] M. Lemoine, K. Murase, and F. Rieger, Nonlinear aspects of stochastic particle acceleration, *Phys. Rev. D* **109**, 063006 (2024).

[44] We determine $\gamma_{\text{max}} = E_{\text{max}}/(mc^2) + 1$ based on the highest energy at which $E_{\text{max}} f(E_{\text{max}})$ is less than a factor of 10^5 below the peak of $E f(E)$.

[45] J. Nättälä and A. M. Beloborodov, Heating of Magnetically Dominated Plasma by Alfvén-Wave Turbulence, *Phys. Rev. Lett.* **128**, 075101 (2022).

[46] C. Vega, S. Boldyrev, and V. Roytershteyn, Anisotropic particle acceleration in alfvénic turbulence, *The Astrophysical Journal* **985**, 231 (2025).

[47] For simplicity, and considering the absence of strong bulk flows, we compute the kinetic and magnetic pressures in the simulation frame, rather than in the proper fluid frame [21]. We confirmed that a more elaborate estimate based on the transformation into the fluid frame leaves results practically unchanged.

[48] M. Goodbred and Y.-H. Liu, First-Principles Theory of the Relativistic Magnetic Reconnection Rate in Astrophysical Pair Plasmas, *Phys. Rev. Lett.* **129**, 265101 (2022).

[49] Y.-H. Liu, M. Hesse, F. Guo, W. Daughton, H. Li, P. A. Cassak, and M. A. Shay, Why does Steady-State Magnetic Reconnection have a Maximum Local Rate of Order 0.1?, *Phys. Rev. Lett.* **118**, 085101 (2017).

[50] Y.-H. Liu, P. Cassak, X. Li, M. Hesse, S.-C. Lin, and K. Genestreti, First-principles theory of the rate of magnetic reconnection in magnetospheric and solar plasmas, *Communications Physics* **5**, 97 (2022).

[51] Eq. (2) is formally derived assuming a cold plasma upstream of the reconnection layer [48]. We adopt it as a crude estimate, given that a more precise expression is not known to us.

[52] M. Hoshino, Energy Partition of Thermal and Nonthermal Particles in Magnetic Reconnection, *The Astrophysical Journal* **946**, 77 (2023).

[53] D. Singh, O. French, F. Guo, and X. Li, Low-energy Injection and Nonthermal Particle Acceleration in Relativistic Magnetic Turbulence, *The Astrophysical Journal* **979**, 39 (2025).

[54] F. Guo, X. Li, O. French, Q. Zhang, W. Daughton, Y.-H. Liu, W. Matthaeus, P. Kilian, G. Johnson, and H. Li, Comment on “Nonideal Fields Solve the Injection Problem in Relativistic Reconnection”, *Phys. Rev. Lett.* **130**, 189501 (2023).

[55] The particle energies are computed in the frame comoving with the drift velocity $c\mathbf{E} \times \mathbf{B}/B^2$ and averaged over the gyration time, to remove high-frequency oscillations.

[56] P. A. Becker, T. Le, and C. D. Dermer, Time-dependent Stochastic Particle Acceleration in Astrophysical Plasmas: Exact Solutions Including Momentum-dependent Escape, *The Astrophysical Journal* **647**, 539 (2006).

[57] O. Porth, S. S. Komissarov, and R. Keppens, Three-dimensional magnetohydrodynamic simulations of the Crab nebula, *Monthly Notices of the Royal Astronomical Society* **438**, 278 (2014).

[58] M. Lyutikov, T. Temim, S. Komissarov, P. Slane, L. Sironi, and L. Comisso, Interpreting Crab Nebula's synchrotron spectrum: two acceleration mechanisms, *Monthly Notices of the Royal Astronomical Society* **489**, 2403 (2019).

[59] S. Xu, N. Klingler, O. Kargaltsev, and B. Zhang, On the Broadband Synchrotron Spectra of Pulsar Wind Nebulae, *Astrophys. J.* **872**, 10 (2019).

[60] L. Comisso, E. Sobacchi, and L. Sironi, Hard Synchrotron Spectra from Magnetically Dominated Plasma Turbulence, *The Astrophysical Journal Letters* **895**, L40 (2020).

[61] N. R. MacDonald and A. P. Marscher, Faraday Conversion in Turbulent Blazar Jets, *Astrophys. J.* **862**, 58 (2018).

[62] E. P. Alves, J. Zrake, and F. Fiúza, Efficient Nonthermal Particle Acceleration by the Kink Instability in Relativistic Jets, *Phys. Rev. Lett.* **121**, 245101 (2018).

[63] J. Davelaar, A. A. Philippov, O. Bromberg, and C. B. Singh, Particle Acceleration in Kink-unstable Jets, *The Astrophysical Journal Letters* **896**, L31 (2020).

[64] F. Bacchini, L. Arzamasskiy, V. Zhdankin, G. R. Werner, M. C. Begelman, and D. A. Uzdensky, Fully Kinetic Shearing-box Simulations of Magnetorotational Turbulence in 2D and 3D. I. Pair Plasmas, *The Astrophysical Journal* **938**, 86 (2022).

[65] F. Bacchini, V. Zhdankin, E. A. Gorbunov, G. R. Werner, L. Arzamasskiy, M. C. Begelman, and D. A. Uzdensky, Collisionless Magnetorotational Turbulence in Pair Plas-

mas: Steady-State Dynamics, Particle Acceleration, and Radiative Cooling, *Phys. Rev. Lett.* **133**, 045202 (2024).

[66] E. A. Gorbunov, F. Bacchini, V. Zhdankin, G. R. Werner, M. C. Begelman, and D. A. Uzdensky, First-principles Measurement of Ion and Electron Energization in Collisionless Accretion Flows, *The Astrophysical Journal Letters* **982**, L28 (2025).

END MATTER

Appendix A: Dependence on δb .—We performed additional simulations at $\sigma_0 = 20$ to check the dependence on the turbulence magnetic fluctuation strength δb . We scale T_0 in proportion to δb^2 , so that T_0 is always below the expected steady-state temperature of the turbulent plasma. As seen from Fig. 4, the efficiency of the non-thermal acceleration is significantly reduced at $\delta b < 1$, in agreement with previous works [22, 23, 26, 27, 45]. We also compute the steady-state plasma β for these runs and compare it to our prediction (1). The result is shown in the inset of Fig. 4. We note the good agreement between our analytic prediction and the simulations.

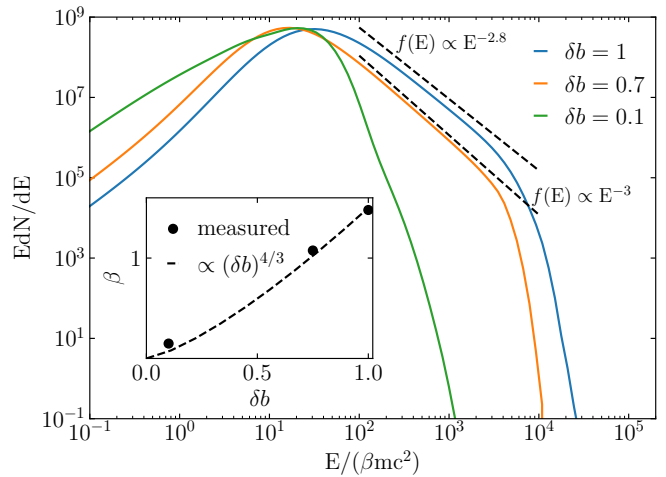


Figure 4. Steady-state particle distributions at different δb . The inset shows the dependence of plasma β on the strength of magnetic-field fluctuations δb . The dashed black curve demonstrates the fit by our analytical formula (1).